

System identification applied to long-span cable-supported bridges using seismic records

Dionysius M. Siringoringo^{*,†,‡} and Yozo Fujino[§]

Department of Civil Engineering, The University of Tokyo, 7-3-1 Hongo, Bunkyo-ku, Tokyo 113-8656 Japan

SUMMARY

This paper presents the application of system identification (SI) to long-span cable-supported bridges using seismic records. The SI method is based on the System Realization using Information Matrix (SRIM) that utilizes correlations between base motions and bridge accelerations to identify coefficient matrices of a state-space model. Numerical simulations using a benchmark cable-stayed bridge demonstrate the advantages of this method in dealing with multiple-input multiple-output (MIMO) data from relatively short seismic records. Important issues related to the effects of sensor arrangement, measurement noise, input inclusion, and the types of input with respect to identification results are also investigated. The method is applied to identify modal parameters of the Yokohama Bay Bridge, Rainbow Bridge, and Tsurumi Fairway Bridge using the records from the 2004 Chuetsu-Niigata earthquake. Comparison of modal parameters with the results of ambient vibration tests, forced vibration tests, and analytical models are presented together with discussions regarding the effects of earthquake excitation amplitude on global and local structural modes. Copyright © 2007 John Wiley & Sons, Ltd.

Received 22 March 2006; Revised 3 August 2007; Accepted 8 August 2007

KEY WORDS: MIMO system identification; seismic response; instrumented bridge; state-space realization; cable-supported bridge

1. INTRODUCTION

The recent growing interest in bridge assessment and monitoring has led to the instrumentation of many bridges in Japan, especially the long-span cable-supported ones. Since most part of Japan is located on a seismically active area, these permanent instrumentation installations provide

*Correspondence to: Dionysius M. Siringoringo, Department of Civil Engineering, The University of Tokyo, Tokyo, Japan.

†E-mail: dion@bridge.t.u-tokyo.ac.jp

‡JSPS Postdoctoral Research Fellow.

§Professor.

Contract/grant sponsor: Japanese Ministry of Education, Culture, Sports, Science and Technology

Contract/grant sponsor: Japan Society for the Promotion of Science (JSPS)

high-quality seismic records every time an earthquake occurs. Such records are essential to gain insights into real behavior of bridges and to evaluate the adequacy of bridge seismic design codes [1].

To assess the dynamic performance of a bridge using measurement data, a procedure named system identification (SI) is implemented. This procedure is an inverse analysis that involves determination of a mathematical model and an estimation of its parameters based on the measured bridge responses. Notable contributions on SI applied to bridge structures can be found in the literature, starting from the type of technique used in the analysis to the evaluation of identification results [2–8]. Most of the work, however, address the SI problems that are based on ambient response. There have been few studies that involve SI subjected to seismic excitation, and among these few, most are applied to short-span bridges [9–11]. This paucity is primarily due to the limited number of seismic records since not until recently have long-span bridges been instrumented with permanent sensors, and not all the currently instrumented bridges are located in seismically active areas. Among the few studies of the SI applied to long-span bridges, the Vincent Thomas suspension bridge has been the subject of extensive research using seismic records from the 1987 Whittier Narrows and the 1994 Northridge earthquakes [12–14].

Although ambient vibration tests (AVTs) provide valuable information for structural identification, verification of analytical models [2–6], and understanding the aerodynamic effect on long-span bridges [7, 8], the small excitations they produce are not always adequate. Observations show that the dynamic performances of the structures are quite different during relatively small excitations of ambient vibration and during stronger excitations such as ground motion. Furthermore, in an effort to improve our understanding of the earthquake-resistant design of long-span bridges, the actual seismic response would be more useful than the dynamic response yielded by other types of excitations. Therefore, there is a strong interest and recognition of the importance of SI using strong motion records.

The work reported here presents case studies of the application of multiple-input multiple-output (MIMO) SI to three long-span bridges in the Tokyo Bay area. The methodology used in this study is based on the System Realization using Information Matrix (SRIM) [15], which utilizes correlations between input–output data for realization of a state-space model and estimation of modal parameters. The method has been successfully implemented for modal testing of a large space-structure system [16] and to a highway bridge system using earthquake records [17]. To provide a comprehensive discussion, this paper includes: (1) a brief explanation of the SI method, (2) numerical verification using a benchmark cable-stayed bridge, (3) application of the SI to the Yokohama Bay Bridge, Rainbow Bridge, and Tsurumi Fairway Bridge using the records from the Chuetsu-Niigata earthquake, and (4) evaluation of identification results.

2. DESCRIPTION OF THE BRIDGES AND SEISMIC RECORDS

2.1. *Description of the bridges*

The first bridge studied is the Yokohama Bay Bridge, located at the entrance of Yokohama harbor (Figure 1(a)). It is a double-deck steel-truss box cable-stayed bridge with a central span of 460 m and two side spans of 200 m each. The bridge, completed in 1988, has two H-shaped towers 172-m high and 29.25-m wide. Eighty-five sensors measuring acceleration and displacement are installed

SYSTEM IDENTIFICATION APPLIED TO LONG-SPAN CABLE-SUPPORTED BRIDGES

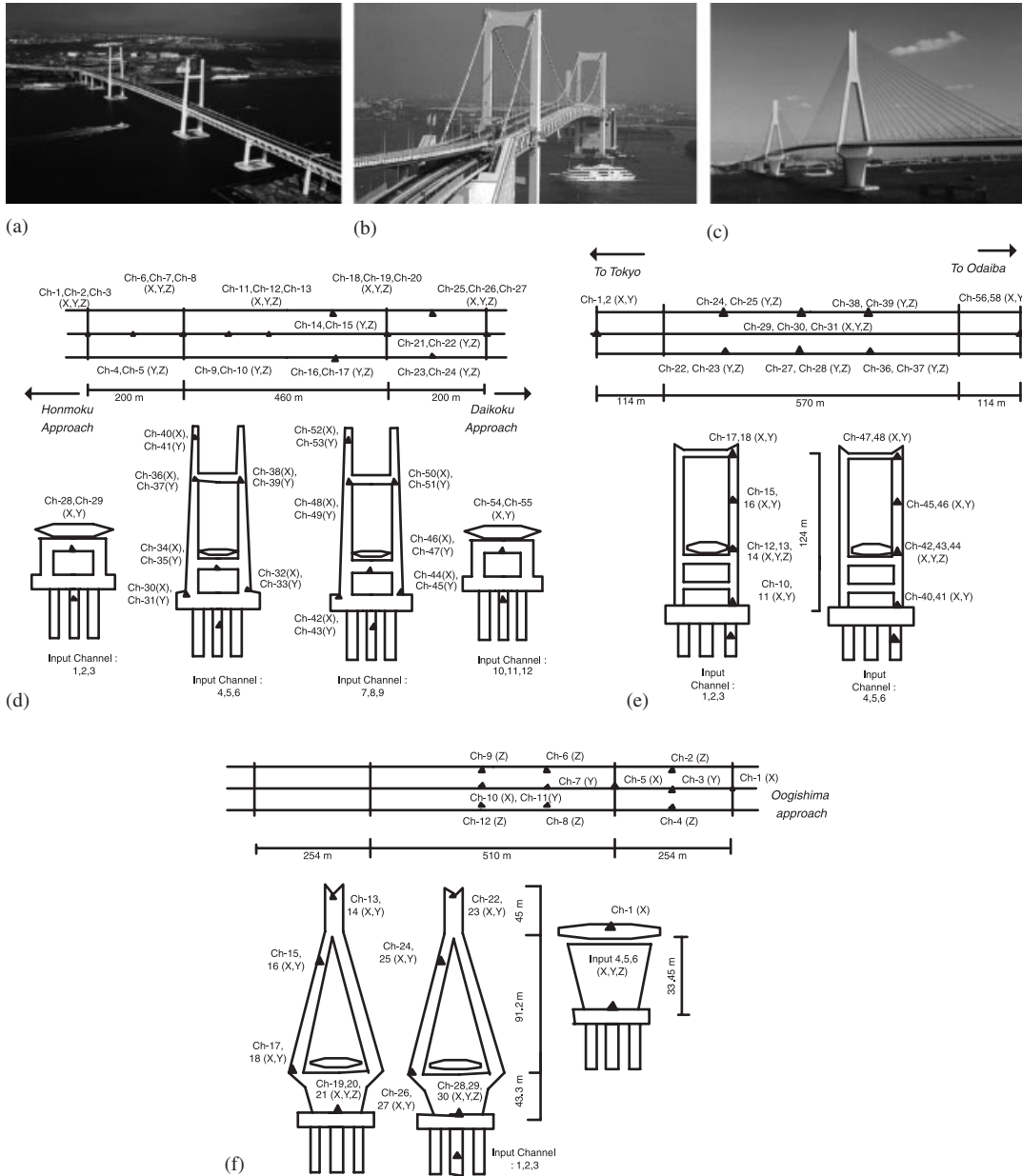


Figure 1. View of the studied bridges: (a) Yokohama Bay Bridge; (b) Rainbow Bridge; and (c) Tsurumi Fairway Bridge. Sensor arrangement for SI of (d) Yokohama Bay Bridge; (e) Rainbow Bridge; and (f) Tsurumi Fairway Bridge.

at 36 locations throughout the bridge. Along the girder, sensors are installed at nine locations with spacing of 115 m (Figure 1(d)). Each sensor has a frequency measurement range from 0.05 to 35 Hz and an accuracy of $15 \times 10^{-3} \text{ amp/cm}^2$.

The second bridge is the Rainbow Bridge, (Figure 1(b)), completed in 1993. It is a double-deck suspension bridge that connects the Shibaura Wharf with Odaiba, Tokyo. The bridge has two H-shaped towers with a height of 125.6 m at the Shibaura side and 124 m at the Odaiba side. The three-spanned girder is composed of a steel truss with side spans of 114 m each and a middle span of 570 m. The upper deck, which is 9.25 m \times 2 m, is used for highway traffic while the lower deck, which is 7 m \times 2 m, is used for a monorail system. The bridge is instrumented with 64 sensors that consist of accelerometers and displacement sensors (Figure 1(e)).

The third bridge is the Tsurumi Fairway Bridge, a three-span single-plane cable-stayed bridge. The girder consists of two 255 m side spans and a 510 m center span. It is characterized by two inverted Y-shaped towers that are each 183-m high and 40-m wide at the bottom. Completed in December 1994, the bridge is currently the longest single-plane cable-stayed bridge in the world. For monitoring purposes, 50 accelerometers are installed on the bridge (Figure 1(f)).

2.2. The 2004 Chuetsu-Niigata Seismic Records

The 23 October 2004, Chuetsu-Niigata strong motions consist of two main shocks recorded at 17:57 (Mj 6.8 according to the Japan Meteorological Agency) and at 18:35 Japan Standard Time (JST). The two main shocks, hereafter named MS1 and MS2, respectively, were followed by two aftershocks. One aftershock was measured at 18:04 on the same day and the other at 10:40 on the next day (named AS1 and AS2, respectively). In application of SI, the records were divided in the following manner.

- For the Yokohama Bay Bridge, the initial 180-s responses of both MS1 and MS2 were divided into three consecutive frames of response with equal time duration of 60 s each, hence MS1-1, MS1-2, MS1-3 and MS2-1, MS2-2, MS2-3, respectively. As a result, along with AS1 and AS2 that also had a duration of 60 s each, eight frames of records were analyzed. The maximum input acceleration of the eight frames varied from 2 to 7 cm/s².
- For the Rainbow Bridge, only the responses from the main shocks were available. They consisted of MS1 (85 s) with a maximum input amplitude of 5.4 cm/s² and MS2 (98 s) with a maximum input amplitude of 4 cm/s².
- For the Tsurumi Fairway Bridge, the records consist of seven frames of 60 s each. They are: MS1, divided into three consecutive frames (i.e. MS1-1, MS1-2, and MS1-3); MS2, divided into two consecutive frames (i.e. MS2-1, MS2-2, and MS2-3); and AS2. The maximum input acceleration varied from 5 to 12 cm/s², where the largest input was recorded during the peak of the MS2 response (i.e. MS2-1).

3. SYSTEM IDENTIFICATION METHODOLOGY

The dynamic behavior of an N degree-of-freedom linear, time-invariant, viscously damped system subjected to earthquake excitation can be presented as a first-order, finite-dimensional, discrete-time, state-variable dynamical system:

$$x(k+1) = \mathbf{A}x(k) + \mathbf{B}z(k) \quad (1a)$$

$$y(k) = \mathbf{R}x(k) + \mathbf{D}z(k) \quad (1b)$$

The quantities of $\mathbf{A} \in \mathbb{R}^{2N \times 2N}$, $\mathbf{B} \in \mathbb{R}^{2N \times q}$, $\mathbf{R} \in \mathbb{R}^{m \times 2N}$, and $\mathbf{D} \in \mathbb{R}^{m \times q}$ are discrete representation of system matrices

$$\begin{aligned} \mathbf{A} &= e^{\mathbf{A}_c \Delta t}, \quad \mathbf{B} = \left[\int_0^{\Delta t} e^{[\mathbf{A}_c] \tau'} d\tau' \mathbf{B}_c \right] \\ \mathbf{R} &= \mathbf{L}[-\mathbf{M}^{-1} \mathbf{K} \quad -\mathbf{M}^{-1} \mathbf{C}], \quad \mathbf{D} = \mathbf{L} \mathbf{M}^{-1} \end{aligned} \quad (2)$$

Matrix $\mathbf{A} \in \mathbb{R}^{2N \times 2N}$ is the system matrix and $\mathbf{B} \in \mathbb{R}^{2N \times q}$ is the input influence matrix, whose continuous-time counterparts are:

$$\mathbf{A}_c = \begin{bmatrix} \mathbf{0} & \mathbf{I} \\ -\mathbf{M}^{-1} \mathbf{K} & -\mathbf{M}^{-1} \mathbf{C} \end{bmatrix}, \quad \mathbf{B}_c = \begin{bmatrix} \mathbf{0} \\ -\mathbf{\Pi} \end{bmatrix} \quad (3)$$

where $x(k)$ is a $2N \times 1$ vector that consists of displacement and velocity. Vector $z(k)$ denotes the $q \times 1$ base motion input recorded from q sensors. Vector $y(k)$ denotes the $m \times 1$ output responses obtained from m sensors of structural accelerations. Matrix $\mathbf{L} \in \mathbb{R}^{m \times 2N}$ is a transformation matrix that connects the position of system's degree-of-freedom with the measured structural output responses. Matrix $\mathbf{\Pi}$ is called the influence matrix that describes the influence of support displacement on the structural displacement. The integer $k=0, 1, 2, \dots, l$ refers to the time-step number, i.e. $x(k+1) = x(k\Delta t + \Delta t)$, with constant Δt that denotes the time interval.

The system matrices \mathbf{A} , \mathbf{B} , \mathbf{R} , and \mathbf{D} in Equation (1) are all unknowns and to be determined from input-output data. Given the responses of p time lengths, Equation (1) can be rewritten in the following matrix form:

$$\mathbf{y}_p(k) = [\mathbf{O}_p] x(k) + [\mathbf{T}_p] \mathbf{z}_p(k) \quad (4)$$

where the $\mathbf{y}_p(k)$, $\mathbf{z}_p(k)$, $[\mathbf{O}_p]$, and $[\mathbf{T}_p]$ are defined as

$$\mathbf{y}_p(k) = [y(k) \quad y(k+1) \quad y(k+2) \quad \dots \quad y(k+p-1)]^T \quad (5a)$$

$$\mathbf{z}_p(k) = [z(k) \quad z(k+1) \quad z(k+2) \quad \dots \quad z(k+p-1)]^T \quad (5b)$$

$$[\mathbf{O}_p] = [\mathbf{R} \quad \mathbf{R} \mathbf{A} \quad \mathbf{R} \mathbf{A}^2 \quad \dots \quad \mathbf{R} \mathbf{A}^{p-1}]^T \quad (5c)$$

$$[\mathbf{T}_p] = \begin{bmatrix} \mathbf{D} & & & & \\ \mathbf{R} \mathbf{B} & \mathbf{D} & & & \\ \mathbf{R} \mathbf{A} \mathbf{B} & \mathbf{R} \mathbf{B} & \mathbf{D} & & \\ \vdots & \vdots & \dots & \ddots & \\ \mathbf{R} \mathbf{A}^{p-2} \mathbf{B} & \mathbf{R} \mathbf{A}^{p-3} \mathbf{B} & \mathbf{R} \mathbf{A}^{p-4} \mathbf{B} & \dots & \mathbf{D} \end{bmatrix} \quad (5d)$$

Matrix $[\mathbf{O}_p] \in \mathbb{R}^{pm \times 2N}$ is the observability matrix and matrix $[\mathbf{T}_p] \in \mathbb{R}^{pm \times pq}$ is a generalized Toeplitz matrix, which is composed by the system's Markov parameters (i.e. $\mathbf{R} \mathbf{A}^{k-1} \mathbf{B}$).

3.1. System Realization using Information Matrix (SRIM)

Let matrix $[\mathbf{O}_p](m+1:pm, :)$ and matrix $[\mathbf{O}_p](1:(p-1)m, :)$ be defined as

$$[\mathbf{O}_p](m+1:pm, :) = [\mathbf{R}\mathbf{A} \ \mathbf{R}\mathbf{A}^2 \ \mathbf{R}\mathbf{A}^3 \ \dots \ \mathbf{R}\mathbf{A}^{p-1}]^T \quad (6a)$$

$$[\mathbf{O}_p](1:(p-1)m, :) = [\mathbf{R} \ \mathbf{R}\mathbf{A} \ \mathbf{R}\mathbf{A}^2 \ \dots \ \mathbf{R}\mathbf{A}^{p-2}]^T \quad (6b)$$

Extracting state matrix \mathbf{A} from Equation (6a) yields

$$\mathbf{A} = [\mathbf{O}_p^*](1:(p-1)m, :)[\mathbf{O}_p](m+1:pm, :) \quad (7)$$

where the asterisk (*) denotes the pseudo-inverse matrix. Following Equations (6) and (7), the integer p should be selected such that matrix $[\mathbf{O}_p](m+1:pm, :)$ has a rank larger than or equal to $2N$, hence $p \geq 2N/m + 1$. Equation (7) states that prior to identification of system matrix \mathbf{A} , one must determine the observability matrix $[\mathbf{O}_p]$. For this purpose, one can expand the vector equation in Equation (4) to

$$[\mathbf{Y}_p](k) = [\mathbf{O}_p]\mathbf{X}(k) + [\mathbf{T}_p][\mathbf{Z}_p](k) \quad (8)$$

where

$$\mathbf{X}(k) = [x(k) \ x(k+1) \ \dots \ x(k+s-1)] \quad (9a)$$

$$[\mathbf{Y}_p] = \begin{bmatrix} y(k) & y(k+1) & \dots & y(k+s-1) \\ y(k+1) & y(k+2) & \dots & y(k+s) \\ \vdots & \vdots & \ddots & \vdots \\ y(k+p-1) & y(k+p) & \dots & y(k+p+s-2) \end{bmatrix} \quad (9b)$$

$$[\mathbf{Z}_p] = \begin{bmatrix} z(k) & z(k+1) & \dots & z(k+s-1) \\ z(k+1) & z(k+2) & \dots & z(k+s) \\ \vdots & \vdots & \ddots & \vdots \\ z(k+p-1) & z(k+p) & \dots & z(k+p+s-2) \end{bmatrix} \quad (9c)$$

Now, let us define the following quantities: \mathbf{R}_{yy} , \mathbf{R}_{zz} , \mathbf{R}_{xx} , \mathbf{R}_{yz} , \mathbf{R}_{yx} , and \mathbf{R}_{xz} as correlations between input (\mathbf{z}), output (\mathbf{y}), and state vector (\mathbf{x}), where the subscripts denote the product of correlation in such a way that the correlation between \mathbf{A}_p and \mathbf{B}_p is defined as $\mathbf{R}_{ab} = (1/s)\mathbf{A}_p(k)\mathbf{B}_p^T(k)$ with integer $s = l - p$ sufficiently large. The observability matrix $[\mathbf{O}_p]$ can be obtained using correlations of input–output matrices:

$$\mathbf{R}_{hh} = [\mathbf{O}_p]\hat{\mathbf{R}}_{xx}[\mathbf{O}_p]^T \quad (10)$$

in which the quantities \mathbf{R}_{hh} and $\hat{\mathbf{R}}_{xx}$ are defined as

$$\mathbf{R}_{hh} = \mathbf{R}_{yy} - \mathbf{R}_{yz}\mathbf{R}_{zz}^{-1}\mathbf{R}_{yz}^T \quad \text{and} \quad \hat{\mathbf{R}}_{xx} = \mathbf{R}_{xx} - \mathbf{R}_{xz}\mathbf{R}_{zz}^{-1}\mathbf{R}_{xz}^T \quad (11)$$

The quantity of \mathbf{R}_{hh} depends only on the input and output correlation matrices, which are all obtained from seismic records.

The solution for matrix $[\mathbf{O}_p]$ in Equation (10) is obtained by factorizing \mathbf{R}_{hh} into three matrices using singular value decomposition. In this decomposition, only the element of the first $pm \times (p-1)m$ size of \mathbf{R}_{hh} matrix is used. Hence, decomposition becomes:

$$\mathbf{R}_{hh}(:, 1:(p-1)m) = \mathbf{H}\Sigma^2\mathbf{V}^T = [\overline{\mathbf{H}}_{2N} \quad \overline{\mathbf{H}}_0] \begin{bmatrix} \Sigma_{2N}^2 & 0_{2N \times n_0} \\ 0_{m_0 \times 2N} & 0_{m_0 \times n_0} \end{bmatrix} \begin{bmatrix} \mathbf{V}_{2N}^T \\ \mathbf{V}_0^T \end{bmatrix} = \overline{\mathbf{H}}_{2N} \Sigma_{2N}^2 \mathbf{V}_{2N}^T \quad (12)$$

In Equation (12), n_0 indicates the number of zero singular values and also the number of columns in \mathbf{V}_0 , whereas m_0 denotes the number of columns in $\overline{\mathbf{H}}_0$ that are orthogonal to the columns in $\overline{\mathbf{H}}_{2N}$. For noise-contaminated data, there are no zero singular values (i.e. $n_0=0$). If no singular values are truncated, $m_0=m$ is the result. In the case where some singular values are truncated, m_0 becomes the sum of whichever the condition of singular value truncation is. Therefore, the decomposition method guarantees that there are at least m columns of $\overline{\mathbf{H}}_0$ that are orthogonal to the columns of $\overline{\mathbf{H}}_{2N}$. As a result, factorization of Equation (10) produces:

$$\mathbf{R}_{hh}[:, 1:(p-1)m] = \overline{\mathbf{H}}_{2N} \Sigma_{2N}^2 \mathbf{V}_{2N}^T = [\mathbf{O}_p] \hat{\mathbf{R}}_{xx} [\mathbf{O}_p]^T[:, 1:(p-1)m] \quad (13)$$

Finally, following the identity in Equation (13), the observability matrix is obtained:

$$[\mathbf{O}_p] = \overline{\mathbf{H}}_{2N} \quad \text{and} \quad \hat{\mathbf{R}}_{xx} [\mathbf{O}_p]^T[:, 1:(p-1)m] = \Sigma_{2N}^2 \mathbf{V}_{2N}^T \quad (14)$$

Given the observability matrix, we can estimate system matrix \mathbf{A} by Equation (7) and matrix \mathbf{R} using Equation (5c). Modal parameters of structural systems are estimated by solving the eigenvalues problem of matrix \mathbf{A} (i.e. $\mathbf{A}\hat{\Phi} = \tilde{\Lambda}\hat{\Phi}$), where $\tilde{\Lambda}$ and $\hat{\Phi}$ denote the eigenvalues and eigenvectors matrix of \mathbf{A} , respectively. Their quantities can be real or complex where, in the latter case, they appear as complex conjugate pairs. The eigenvalues $\tilde{\lambda}_i$ are expressed in z -domain. Hence, they can be related to modal characteristics using the following transformation: $\lambda_i = \ln(\tilde{\lambda}_i)/\Delta t$. Finally, the natural frequency (ω_i) and damping ratio (ξ_i) become:

$$\omega_i = \sqrt{\text{Re}(\lambda_i)^2 + \text{Im}(\lambda_i)^2}, \quad \xi_i = \frac{-\text{Re}(\lambda_i)}{\omega_i} \quad (15)$$

To obtain the mode shapes, eigenvectors in z -domain are transformed into coordinate domain using the relation: $\Phi = \mathbf{R}\hat{\Phi}$.

4. NUMERICAL VERIFICATION

In order to validate the SI method, numerical simulations using a fictitious three-dimensional finite element model of a cable-stayed bridge (Figure 2) were performed. The model includes 177 nodes, 303 frame and cable elements, and linear links that connect both the tower and the end pier to the girder. A damping matrix was computed using the proportional damping with a modal damping ratio of 2% assigned to all modes. The linear model was deemed adequate for this simulation, considering that the center span of the bridge model is less than 425 m (as was concluded in [18]).

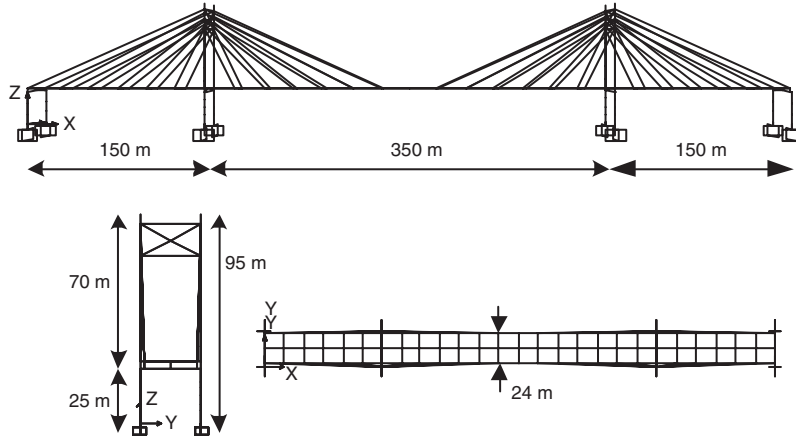


Figure 2. Model of the cable-stayed bridge used in numerical simulation.

4.1. Input signal generation

Three directional artificial ground motions were generated for input signals using filtered shot noise with a prescribed power spectral density of the Kanai–Tajimi (KT) [19] spectrum:

$$S(\omega) = S_0 \frac{\omega_g^4 + 4\omega_g^2 \zeta_g^2 \omega^2}{(\omega^2 - \omega_g^2)^2 + 4\omega_g^2 \zeta_g^2 \omega^2} \quad (16)$$

in which ω_g and ζ_g are the constants that represent the frequency and damping coefficients, respectively. Kanai and Tajimi suggested the values of $\omega_g = 5\pi$ and $\zeta_g = 0.6$ for modeling ground acceleration response during an earthquake. To obtain the amplitude of acceleration, a time-domain intensity modulation function $I(t)$ is employed under the following conditions: (1) $I(t) = I_0(t/t_1)^2$, for $0 < t < t_1$, (2) $I(t) = I_0$ for $t_1 < t < t_2$, and (3) $I(t) = I_0 \exp\{-a(t - t_2)/t_0\}$ for $t_2 > t$, with $t_1 = 0.7t_0$, $t_2 = 1.15t_0$, and $a = 0.8$, where t_0 denotes the duration of the strong motion. The KT spectrum is utilized to generate artificial ground motions in order to better represent the frequency content of seismic excitations especially at a low-frequency range (0–10 Hz). At this range, the KT spectrum can capture the frequency characteristics similar to the ones discovered from real ground motions. Therefore, by using the KT spectrum, one can create a representative artificial ground motion that contains the same characteristics of real ground motions and, at the same time, define its amplitude, duration, and the peak location by selecting and scaling the intensity modulation and the duration function.

Triaxial input accelerations were applied at the bottom of both towers and end piers using a sampling frequency of 100 Hz and a duration of 60 s. Dynamic responses of the bridge were calculated by the modal superposition method using the first 50 modes. To simulate the actual measurement conditions, random white noise was added to the responses to achieve a noise-to-signal ratio of 10%, defined as the ratio of the root mean square (RMS) of noise and the actual acceleration data at each node. Furthermore, to investigate the effect of the number of output sensors and their positions with respect to the identification results, nine sets of data were used in the analysis. Initially, three sets of sensor configurations were analyzed: (1) system of 21 sensors

(i.e. nine sensors from girders, six sensors from piers, and six from towers), (2) system of nine girder sensors, and (3) system of three girder sensors. Further, for each of these sensor configurations, three sets of systems were analyzed, namely, the vertical, transverse, and longitudinal systems.

4.2. Realization of global modes

As mentioned in Equation (7), the total number of identified modes depends on the size of matrix \mathbf{A} , which is determined from the number of singular values of \mathbf{R}_{hh} (Equations (13) and (14)). Large singular values represent the strength of the dominating modes, while the small ones consist of either noise or fictitious computational modes. After the small singular values during decomposition of \mathbf{R}_{hh} are excluded, matrix \mathbf{A} is realized. At this point, the crucial step is the selection of a singular value cutoff. In an ideal no-noise measurement, the cutoff value can be determined by observing a sudden drop in a singular value plot. In actual practice, however, no such case exists. The inevitable presence of noise and small nonlinearity could distort the system to some extent and, as a result, no typical sudden drop exists. Consequently, distinguishing a real mode from computation modes requires a modal selection technique. In this study, a technique that selects a set of modes by assigning threshold values and mode selection using logic operators is implemented.

Initially, all modes are generated using a specified singular value cutoff (usually the value that corresponds to a very small singular value is selected). The resulting modes are further evaluated by employing the following threshold criteria:

1. Modes with a negative damping ratio and/or an uncharacteristically high damping ratio are disqualified. It was found from numerical simulation that many false modes caused by noise or small nonlinearity have the characteristics of negative damping and/or uncharacteristically high damping.
2. Modes with an Extended Modal Assurance Criteria of the Observability Matrix (EMACO) value of less than 0.8 are omitted. The EMACO index [20] computes the degree of coherence and consistency of the mode in an observability matrix. Its value varies from 0.0 to 1.0. The more consistent one mode appears in the observability matrix, the closer its EMACO value is to unity.
3. In cases when SI generates two or more similar modes having frequencies very close to each other (for example, within 5% of each other), and when these modes have close Modal Assurance Criteria (MAC) values, then only the mode that has the highest EMACO value is selected as the representative mode.

To better understand the procedure, one can refer to the example given in Figure 3. This figure shows the SI results of a benchmark model using 21 output sensors and 10% noise. In Figure 3(a), one can observe that singular values beyond 150 are almost zero. Therefore, 150 is selected as the cutoff value. This means the total number of modes obtained is $\frac{150}{2} = 75$ since they all appear in conjugate frequencies. The first selection is made by observing the values of the damping ratios (Figure 3(b)). Of these 75 modes, 25 modes were disqualified upon evaluating the damping ratios as imposed by the first set of threshold criteria (Figure 3(c)). Further selection using the second set of criteria results in 44 modes that have EMACO values greater than 0.8 (Figure 3(d)). Finally, 38 modes were selected after excluding six more modes according to the third set of threshold criteria.

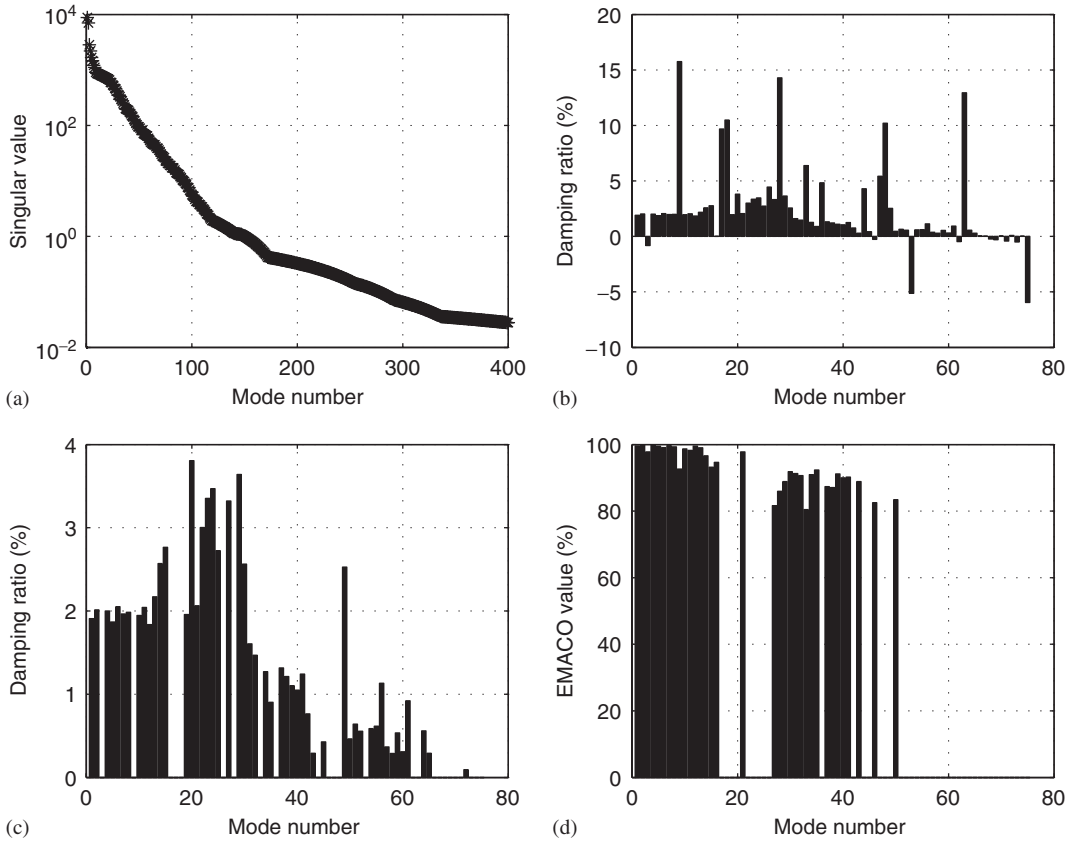


Figure 3. Simulation results of the cable-stayed bridge models: (a) typical singular value plot with the number of modes generated (the number of modes includes the complex conjugate); (b) the corresponding damping ratio of the first batch; (c) selected modes after removing the modes with unacceptable damping ratios; and (d) selected modes after removing modes with unacceptable EMACO values. [Note: Mode number is in the order according to the singular values].

4.3. Results of numerical simulation

Table I lists the results of identification (for brevity only the first 15 modes are listed) quantified by the following error indicator:

$$\omega_{\text{error}}, \zeta_{\text{error}} = \left| \frac{(\omega_{\text{est}}, \zeta_{\text{est}}) - (\omega_{\text{act}}, \zeta_{\text{act}})}{(\omega_{\text{act}}, \zeta_{\text{act}})} \right| \times 100\% \quad (17)$$

It is evident from Table I that SI performs very well in capturing modes even when the number of sensors used is smaller compared with the total number of degrees of freedom. If 21 sensors are used, 38 out of 50 low-order modes can be accurately identified. The errors of natural frequency estimates are less than 2%, while the errors of damping estimates reach the maximum of 10%. If nine sensors are used, most of the vertical, lateral, and torsion modes can be clearly identified. The results also show that if only three sensors from the girders are used, six first vertical modes can

SYSTEM IDENTIFICATION APPLIED TO LONG-SPAN CABLE-SUPPORTED BRIDGES

Table I. (a) Identified natural frequencies, (b) Identified damping ratios, and (c) Identified MAC values of the cable-stayed bridge model subjected to Kanai–Tajimi ground motion.

Real value	21 sensors		9 sensors		3 sensors		Mode type
	No noise	Added	No noise	Added	No noise	Added	
<i>(a) Identified frequency (Hz)*</i>							
0.34	0.34 [0.00]	0.34 [0.14]	0.34 [0.14]	0.34 [0.00]	0.34 [0.00]	0.34 [0.14]	1st V.S
0.41	0.41 [0.00]	0.41 [0.01]	0.41 [0.24]	0.41 [0.00]	0.41 [0.22]	0.41 [0.24]	2nd V.A
0.42	0.42 [0.00]	0.42 [0.02]	0.42 [0.77]	0.42 [1.49]	0.42 [0.19]	0.42 [1.49]	1st T
0.56	0.56 [0.00]	0.56 [0.03]	0.56 [0.20]	0.56 [0.20]	—	—	1st Tor
0.61	0.61 [0.00]	0.61 [0.18]	0.61 [0.18]	—	—	—	2nd Tor
0.64	0.64 [0.07]	0.64 [0.07]	0.64 [0.00]	0.64 [0.07]	—	—	1st L
0.70	0.70 [0.07]	0.70 [0.07]	0.70 [0.00]	0.69 [1.36]	0.70 [0.07]	0.71 [1.05]	3rd V.S
0.76	0.76 [0.00]	0.77 [0.01]	0.76 [0.64]	—	—	—	3rd Tor
0.82	0.82 [0.20]	0.82 [0.20]	0.82 [0.32]	0.82 [0.20]	—	—	Tw. Op
0.83	0.83 [0.00]	0.83 [0.00]	0.83 [0.00]	0.83 [0.00]	—	—	Tw Ip
0.92	0.92 [0.00]	0.92 [0.07]	0.92 [0.04]	0.92 [0.04]	0.92 [0.10]	—	4th V.A
1.02	1.02 [0.00]	1.02 [0.48]	1.02 [0.48]	1.03 [0.01]	1.03 [0.01]	1.02 [0.09]	5th V.S.
1.12	1.12 [0.02]	1.12 [0.01]	1.12 [0.08]	—	—	—	4th Tor
1.22	1.22 [0.00]	1.22 [0.09]	1.22 [0.00]	1.22 [0.00]	1.25 [2.55]	1.23 [0.83]	6th V.A.
1.27	1.27 [0.00]	1.27 [0.00]	1.27 [0.00]	1.27 [0.13]	1.27 [0.02]	—	7th V.S
<i>(b) Identified damping ratio (%)*</i>							
2.00	2.00 [0.00]	2.00 [0.00]	2.00 [0.06]	2.00 [0.11]	2.00 [0.06]	1.58 [21.00]	1st V.S
2.00	2.00 [0.00]	2.00 [0.00]	2.00 [0.00]	2.00 [0.00]	4.66 [133.00]	5.14 [156.85]	2nd V.A
2.00	2.00 [0.05]	2.00 [0.00]	2.00 [0.00]	2.00 [0.00]	2.00 [0.00]	2.00 [0.00]	1st T
2.00	2.00 [0.00]	2.00 [0.00]	2.00 [0.00]	2.00 [0.00]	—	—	1st Tor
2.00	2.00 [0.00]	2.00 [0.00]	2.00 [0.00]	—	—	—	2nd Tor
2.00	2.00 [0.00]	2.00 [0.00]	2.00 [0.00]	2.00 [0.00]	—	—	1st L
2.00	2.00 [0.00]	2.00 [0.00]	2.00 [0.02]	1.99 [0.50]	2.00 [0.02]	1.78 [10.90]	3rd V.S
2.00	2.00 [0.00]	2.00 [0.05]	2.00 [0.00]	—	—	—	3rd Tor
2.00	2.00 [0.00]	2.00 [0.00]	2.01 [0.15]	1.94 [3.00]	—	—	Tw. Ap
2.00	2.00 [0.00]	2.00 [0.00]	2.30 [15.50]	3.57 [78.50]	—	—	Tw Ip
2.00	2.00 [0.00]	2.10 [5.00]	2.00 [0.05]	2.00 [0.00]	1.95 [4.10]	—	4th V.A
2.00	2.00 [0.00]	2.00 [0.00]	2.00 [0.02]	2.00 [0.00]	6.13 [206.50]	1.88 [6.10]	5th V.S.
2.00	1.92 [4.05]	1.91 [4.50]	2.00 [0.00]	—	—	—	4th Tor
2.00	2.00 [0.00]	2.00 [0.00]	2.00 [0.00]	2.00 [0.00]	2.01 [0.50]	2.94 [46.75]	6th V.A.
2.00	2.00 [0.00]	2.00 [0.00]	2.01 [0.15]	1.99 [0.50]	2.10 [4.98]	—	7th V.S
<i>(c) MAC Values (%)</i>							
21 sensors		9 sensors					
No noise	Added	No noise	Added			Mode type	
99.4	94.0	99.2	92.0			1st V.S	
98.1	99.1	98.3	91.5			2nd V.A	
98.5	92.3	97.4	94.2			1st T	
96.8	90.7	98.3	95.6			1st Tor	
91.7	92.0	94.5	—			2nd Tor	
97.4	90.4	90.7	89.1			1st L	
97.0	93.5	97.0	90.7			3rd V.S	

Table I. *Continued.*

21 sensors		9 sensors		Mode type
No noise	Added	No noise	Added	
96.5	97.7	93.3	—	3rd Tor
92.3	90.1	90.6	90.8	Tw. Ap
93.2	94.2	93.4	92.1	Tw Ip
92.5	93.1	92.0	91.4	4th V.A
99.0	90.3	93.7	90.2	5th V.S.
92.4	90.4	92.1	—	4th Tor
94.1	92.2	95.0	93.2	6th V.A.
97.5	91.3	97.9	91.3	7th V.S

Note: S: Symmetric; A: asymmetric; V: vertical; T: transverse; L: longitudinal; Tw: tower; Op: out of phase; Ip: in phase; Tor: torsional.

*Value in bracket indicates error in (%).

still be identified. It should be noted, however, that the accuracy of damping estimates decreases sharply when fewer sensors are used.

Table I(c) shows that the MAC values of identified modes are all about 90%, suggesting a high degree of coherency between identified mode shapes and the FEM modes. Owing to the limitation of shapes, only the MAC values from measurement with 21 and 9 sensors are listed. In the case of measurement with three sensors, some modes have similar patterns but were identified at different frequencies. These results are reasonable, considering the limitation of sensor position. There is no general trend on how measurement with fewer sensors would affect the MAC values. For no-noise measurement, it appears that the MAC values decrease when the number of sensors is reduced. This, however, was not very obvious in the case of noise-added measurement. For an equal number of sensors, the presence of noise generally reduced the accuracy of mode shape estimates, as evidenced by the reduction in MAC values. However, great care should be taken when drawing conclusions regarding the value of MAC and errors of mode shape. Since the MAC index does not identify the source of the error, it is possible that a large difference in a single location can cause a large error in the index, which could be misinterpreted as a significant error in the shape of the entire mode. Nevertheless, the essential outcome of this simulation is the fact that in the case of realistic noise-contaminated measurement using a limited number of sensors, the SI method used in this study still achieves good results in capturing modes, as evidenced by the high values of MAC.

The short duration of an earthquake record can generally create problems especially during estimation of the damping ratio. This effect becomes obvious when one selects the appropriate p -value before assembling the information matrix. Theoretically, the minimum value of $p \geq 2N/m + 1$ guarantees an exact solution. However, due to the presence of measurement noise, the actual minimum p -value was found to be larger than the theoretical one. Figures 4(a) and (b) show examples of error accumulation found in the identification of vertical modes with respect to the selection of the p -value. It can be seen that in the cases of added noise and fewer sensors, larger p -values give a better estimation of modal parameters. In all cases of sensor configurations, it was found that the estimates converge to certain values of p , from which the best estimates of modal parameters are obtained.

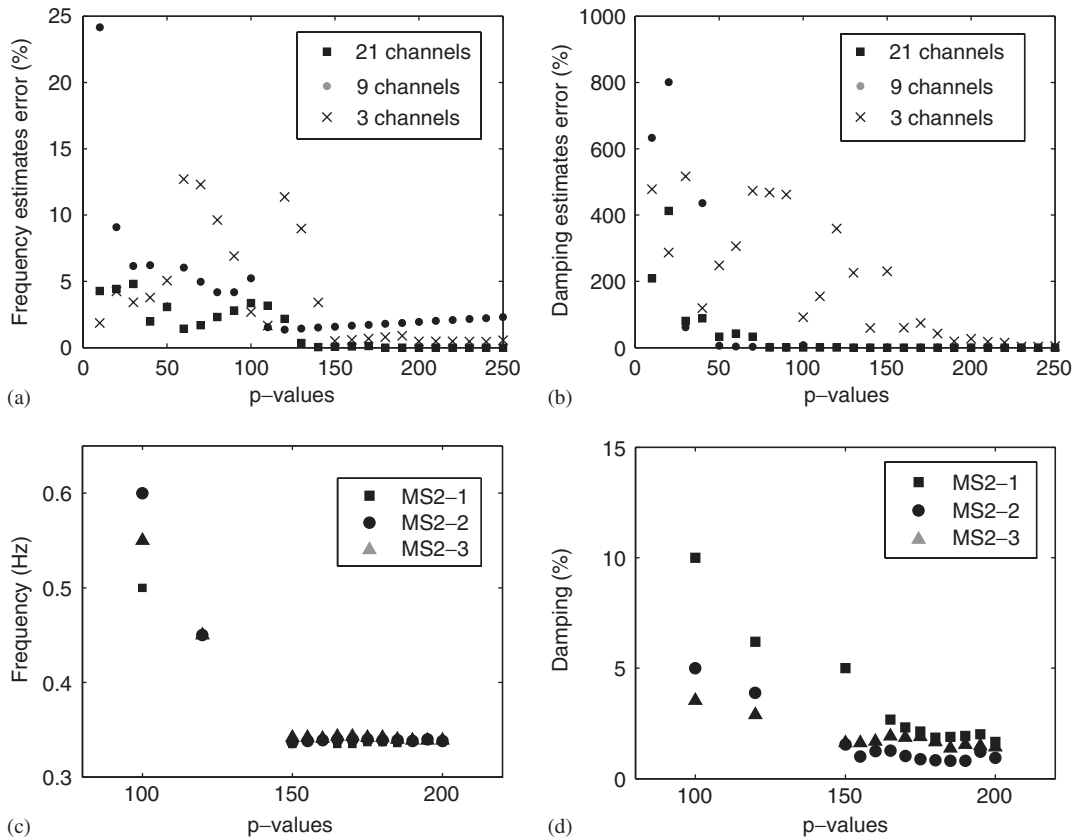


Figure 4. Consistency of modal parameters with respect to the selection of p -values for numerical simulation using cable-stayed bridge model: (a) frequency estimates and (b) damping ratio estimates. Identification results of the first vertical mode of Yokohama Bay Bridge (MS2 response): (c) natural frequencies and (d) damping ratios.

4.4. Influence of input inclusion and excitation type

The SRIM method is principally based on the assumption that the responses are ergodic or at least weakly stationary. It is therefore important to investigate the performance of SI under conditions that do not follow this assumption. In addition, the SRIM method also allows exclusion of input when computing an information matrix (\mathbf{R}_{hh}), which yields to the case of the output-only SI (i.e. $\mathbf{R}_{hh} = \mathbf{R}_{yy}$). To investigate the effects of input inclusion as well as the types of inputs, numerical simulations were performed using three types of input excitations, namely, the Broadband Stationary Gaussian input (BSI), the Narrowband Stationary Gaussian input (NSI) with low-pass frequency of 10 Hz, and the Narrowband Nonstationary random input (NNI).

Figure 5 summarizes the effect of input inclusion in terms of error accumulation in identifying the first six vertical modes. It can be observed that in the case of the input-output scheme, the natural frequency estimates are accurate regardless of the types of inputs, as indicated by the error that was below 1% (Figure 5(a)). In this scheme, accuracy is much better when the input

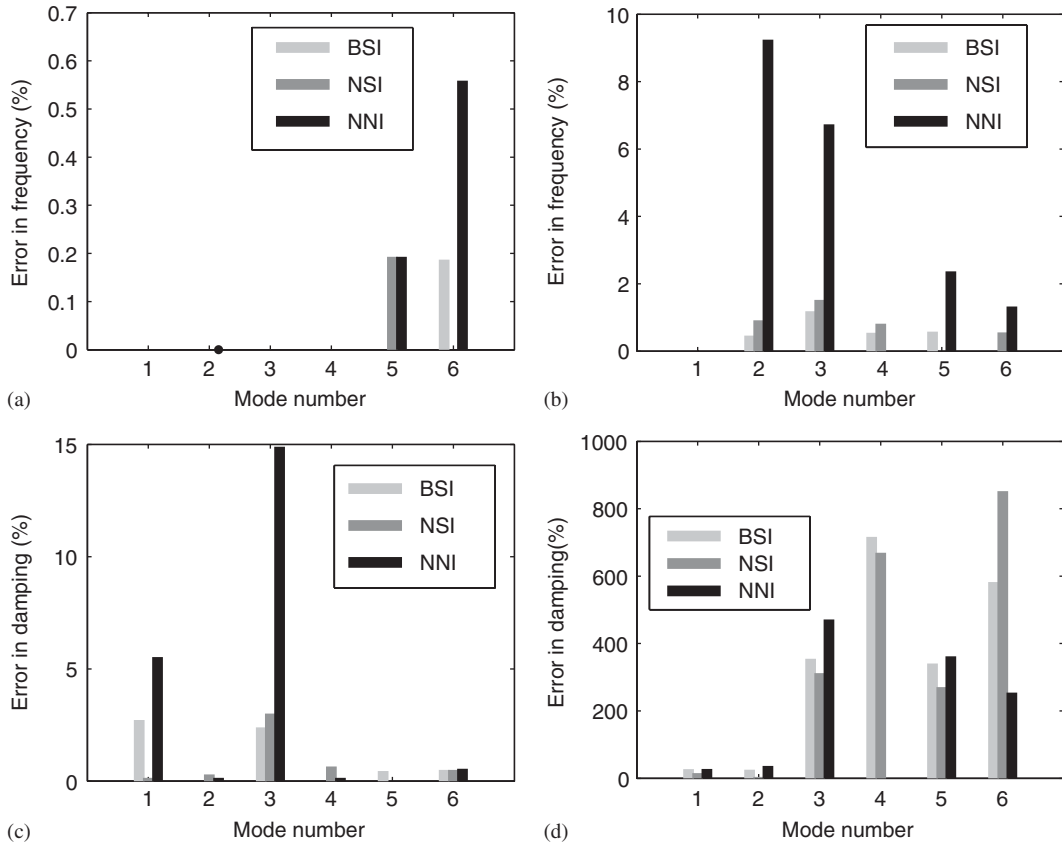


Figure 5. Comparison of errors in modal parameters of the first six vertical modes with respect to input inclusion and type of input: (a) frequency estimates of input–output scheme; (b) frequency estimates of output-only scheme; (c) damping estimates of input–output scheme; and (d) damping estimates of output-only scheme. Note: BSI, Broadband Stationary Gaussian Random Input; NSI, Narrowband Stationary Gaussian Random Input with low-pass frequency of 10Hz, and NNI, Narrowband Nonstationary Random Input.

is broadband white noise. Errors in damping estimates are larger when the system is subjected to narrowband nonstationary excitation (Figure 5(c)). The scheme of SI using only output response gives relatively accurate results for natural frequency estimates (Figure 5(b)) but not for damping estimates (Figure 5(d)). In the output-only case, the frequency estimates are again much better when the input is broadband stationary white noise than when it is nonstationary.

These results emphasize the importance of input inclusion when using this SI method. In a case where excitation is a broadband stationary random process, input inclusion may be considered optional, although a longer record is necessary to obtain the best result. In the case of an earthquake where (1) inputs are rarely as rich in frequency as broadband white noise, (2) inputs are mostly nonstationary, and (3) records are relatively short, the SI must be performed by including input in the information matrix. This would give better estimates of modal parameters.

5. APPLICATION OF SYSTEM IDENTIFICATION

To effectively implement the identification method, three sets of input–output data (i.e. longitudinal, vertical, and transverse) representing the three types of bridge motions were studied (Table II). As inputs, responses from triaxial accelerometers located at the bottoms of the towers and the end piers were selected (Figure 1). Instead of the free-field responses, these responses were utilized to minimize the effect of soil–structure interaction.

5.1. Results of the Yokohama Bay Bridge

In order to study the sensitivity of modal parameters with respect to the length of input–output in block matrices ($[\mathbf{Y}_p]$ and $[\mathbf{Z}_p]$), several records with various lengths were evaluated. This was done by varying the number of rows of both $[\mathbf{Y}_p]$ and $[\mathbf{Z}_p]$, while the number of columns was set at 5500. Modal parameters were calculated separately for these different block matrices. Observation of modal parameters for various p -values shows that they converge into constant values. Figures 4(c) and (d) show that both natural frequency and damping ratio converge to constant values when $p=200$. Therefore, this value was selected as the representative p -value for the analysis.

Fifteen modes within the frequency range of 0.1–2.5 Hz were identified (Table III). The lowest mode was identified at 0.11 Hz, which was a typical first longitudinal mode when compared with the FEM modes. In the vertical system, five bending modes and three torsion modes were identified. In the transverse system, six modes were identified of which the first three were identified within the frequency range of 0.28–0.43 Hz. These three modes exhibited similar modal displacement of the girder portion but different modal displacement of the towers. In the first mode, both towers were in phase with each other and also with the girder's transverse motion, whereas in the second mode they were in phase with each other but out of phase with the girder.

Table III lists the identified mode shapes together with the results of FEM as well as the AVT and the forced vibration test (FVT)—both were performed immediately after completion of the structure [21]. It can be observed that the identified frequencies are in good agreement with FEM and also with those identified from the tests. The MAC values, calculated between the identified modes and their FEM counterparts, all show values around 90%, suggesting the accuracy of the mode shape estimates. Note also that several modes, which were not excited during either AVT or FVT, can be identified from the earthquake records. They are the first longitudinal mode, the higher vertical modes (i.e. second symmetric and third asymmetric bending mode), and two torsional

Table II. Output sensor arrangement for SI at the three bridges.

System	Yokohama Bay Bridge	Rainbow Bridge	Tsurumi Fairway Bridge
Longitudinal	Ch1X until Ch25X (girder)	Ch1X, Ch12X, Ch29X,	Ch1X, Ch5X, Ch10X (girder)
	Ch30X until Ch49X (towers)	Ch42X and Ch56X (girder)	Ch13X until Ch28X (towers)
	Ch28X until Ch54 X (piers)	Ch10X until Ch47X (tower)	
Vertical	Ch3Z until Ch27Z (girder)	Ch23Z until Ch39Z (girder)	Ch2Z until Ch12Z (girder)
	Ch30X until Ch50X (towers)	Ch10X until Ch47X (towers)	Ch13X until Ch28X (towers)
Transverse	Ch2Y until Ch26Y (girder)	Ch2Y, Ch58Y, Ch 13Y, Ch43Y,	Ch3Y until Ch11Y (girder)
	Ch31Y until Ch51Y (towers)	Ch23Y until Ch38Y (girder)	Ch14Y until Ch29Y (towers)
		Ch11Y until Ch48Y (tower)	

Note: The inputs are shown in Figures 1(c)–(e).

Table III. Identified natural frequencies and damping ratios of Yokohama Bay Bridge from MS1-1 of the Chuetsu-Niigata earthquake and comparisons with results from other tests.

Mode	Natural frequency (Hz)					Damping (%)
	MS1-1 [MAC]*	1990 earthquake [23]	FEM	AVT [21]	FVT [21]	MS1-1 [MAC]*
<i>Longitudinal</i>						
1st Longitudinal mode	0.11 [90%]	0.13	0.14	—	—	3.50
<i>Vertical</i>						
1st Sym. bending	0.35 [96%]	0.36	0.34	0.36	0.34–0.35	2.87
1st Asym. bending	0.53 [94%]	0.55	0.49	0.60	0.54–0.57	4.13
2nd Sym. bending	0.79 [99%]	0.81	0.77	0.85	0.80	1.69
2nd Asym. bending	0.95 [92%]	1.01	1.22	1.01	—	1.61
3rd Sym. Bending	1.14 [N/A]	1.21	N/A	—	—	2.32
1st Torsion	0.86 [92%]	0.86	0.95	0.88	—	0.95
2nd Torsion	1.34 [N/A]	1.38	N/A	—	—	3.31
3rd Torsion	2.50 [N/A]	2.46	N/A	—	—	3.40
<i>Transverse</i>						
1st Sym. tower-girder in phase	0.29 [92%]	0.30	0.28	0.27	—	4.29
1st Sym. tower-girder out of phase	0.43 [N/A]	0.42	N/A	—	—	5.02
1st Asym. towers out of phase	0.38 [96%]	0.39	0.42	0.38	—	5.10
1st Asym. tower-girder out of phase	0.75 [91%]	0.75	0.70	0.68	—	3.99
1st Asym. tower in phase	0.91 [N/A]	0.94	N/A	—	—	4.70
2nd Sym. bending	1.04 [89%]	1.06	1.08	—	—	2.07

Note: N/A: not available; — : not identified.

*Value in [] denotes the MAC value between identified modes and their FEM counterparts.

modes. Considering that the level of excitation of earthquake vibration is much higher than that of ambient vibration, these results are reasonable. Therefore, this fact suggests that seismic records can be used for practical modal analysis in addition to the AVT and the FVT.

Damping ratios were estimated within the range of 0.5–5.1%. Higher damping ratios were observed in the transverse modes, especially during the main shocks. Most of damping ratios of the vertical modes were within 1–4%. These values are higher than those previously estimated (around 2%) during the AVT and FVT [21]. The damping estimates of the torsion modes were found to be lower than the other two motions, with an average of 0–3.5%. The damping estimates of the first torsion mode were especially low (less than 1%).

Figure 6 illustrates some of the mode shapes. It should be noted that the girder vertical modes are represented together with the tower longitudinal modes since the two structural components are coupled in such motion. Similarly, the girder transverse dominant modes are represented together with the tower transverse motion. Owing to selection of the above systems, the girder vertical modes do not include any transverse components. However, the results of numerical simulations show that if a mode is uncoupled in vertical and transverse directions—such as the case of the torsional mode—or if the motion in one direction is slightly more dominant than motions in other directions, then the mode will appear in both vertical and transverse system having identical natural frequency and damping ratio. However, in exception to the torsional modes, this was not the case with the Yokohama Bay Bridge. It was found that the modes that appeared in the vertical direction did not reappear during identification in the transverse direction. To better observe a mode and its motion in all directions, a scheme of a three-dimensional identification system should be employed.

SYSTEM IDENTIFICATION APPLIED TO LONG-SPAN CABLE-SUPPORTED BRIDGES

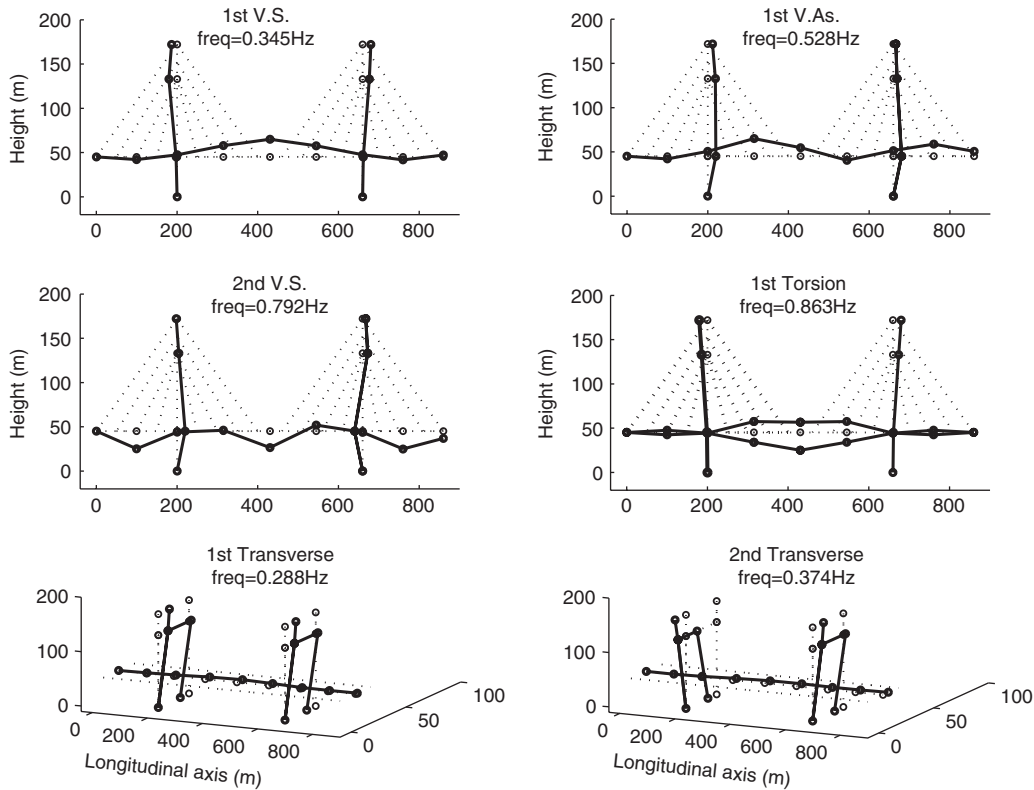


Figure 6. Mode shapes of Yokohama Bay Bridge identified from MS1 (V=Vertical, S=Symmetric, As=Asymmetric).

An example of a relevant study of identification using a three-dimensional system is presented in Reference [22].

Before the 2004 Chuetsu-Niigata earthquake, six significant earthquakes from 1990 to 1997 were recorded on the bridge. The results of their SI were summarized in Reference [23]. The range of the maximum input amplitude of these six earthquakes (i.e. from 2 to 13 cm/s²) is comparable with the range of the maximum input amplitude of the present records. However, the frequencies identified from the six earthquakes are substantially higher than the results from the 2004 Chuetsu-Niigata earthquake (Figure 7). The decreases in frequencies are between 3 and 7% for the vertical modes, 0.8 and 6% for the transverse modes, and around 3% for the torsion modes. These changes are significant and imply that the structural properties might have changed. Considering that the Chuetsu-Niigata earthquake occurred when the construction of an additional deck had been completed, the decrease might indicate that the new deck contributed in large measure as added mass rather than as added stiffness to the whole structure system.

5.2. Results of the Rainbow Bridge

Table IV lists the 13 modes identified from the Rainbow Bridge. Except for the first vertical asymmetric mode, all modes have MAC values around 90%, suggesting consistency and accuracy

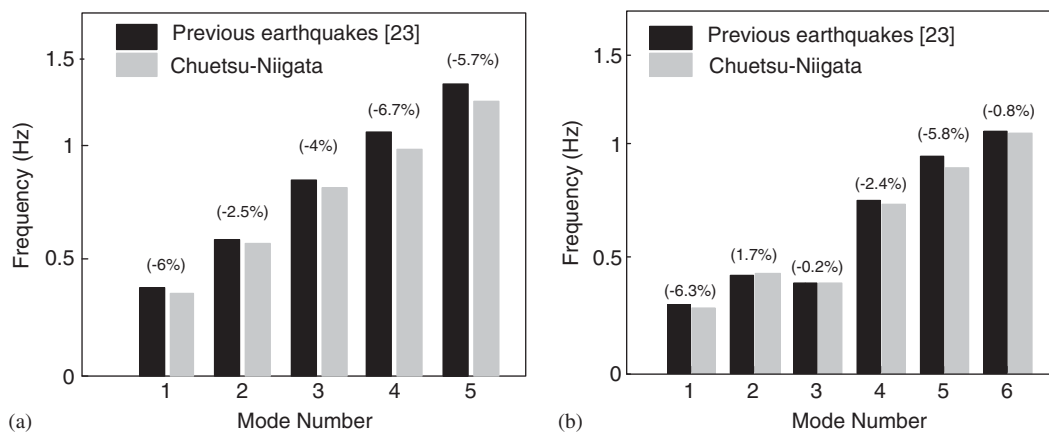


Figure 7. Comparison of natural frequency identified from previous earthquakes and from the 2004 Chuetsu-Niigata earthquake: (a) vertical mode and (b) transverse mode. Note: values in brackets indicate the difference with negative values for decrease.

between the identification results and the FEM results. In the longitudinal motion, the first mode was a swing mode identified at 0.67 Hz. In the vertical motion, eight modes were identified consisting of five bending and three torsion modes. In the transverse direction, four modes were identified.

The first vertical mode is an asymmetric bending. The FEM predicts this mode at a frequency of 0.18 and 0.24 Hz for a hinge model and a fixed model, respectively, with one stationary point located at the exact midpoint of the deck (Figure 8(a)). Identification results revealed similar modes but with slightly different characteristics. These modes were identified at 0.24–0.25 Hz with some influences of the symmetrical mode that caused the stationary point to shift slightly left to the Tokyo side from the girder midpoint. One might be skeptical about this mode, especially after looking at the shape and the fact that it was identified in such a closely spaced frequency with its symmetrical counterpart. However, we decided to include this mode as an identification result after observing the consistency of the mode and after comparing it with the previous FVT results, where a very similar mode was also identified [24].

The first transverse mode, identified at 0.12 Hz, exhibits an in-phase motion of both towers and girder. In the first mode, the girder shows a typical first symmetrical transverse motion, while in the second mode, it shows a typical first asymmetric motion with both towers being out of phase. Several other higher modes were identified. However, due to limitations of the sensor positions, the exact shape of these modes cannot be precisely confirmed.

For comparison, two analytical models were investigated (Figure 8(e)). One model assumed a hinge connection between tower and girder that allowed rotational and longitudinal movement during extensive vibration. The other model assumed a rigid or fixed connection, provided that the friction between the girder and tower connection restrained the longitudinal movement of the girder. The difference in the two models became visible at the first vertical asymmetric mode, where the change from fixed to hinge connection resulted in a 28% reduction of natural frequency. Measurement results during AVT and FVT [24] suggested that the bridge was actually more rigid than it was in either model. Comparing the ratio between the identified values and the

SYSTEM IDENTIFICATION APPLIED TO LONG-SPAN CABLE-SUPPORTED BRIDGES

Table IV. Identified natural frequencies and damping ratios of the Rainbow Bridge from the main shocks of the Chuetsu-Niigata earthquake and comparisons with results from other tests.

Mode	Natural frequency (Hz)						Modal damping ratio (%)		
	SI results		FVT [24]	AVT [24]	FEM		SI results		
	MS1*	MS2*			Hinge model	Fixed model	MS1*	MS2*	AVT [24]
<i>Vertical</i>									
1st Asym. bending	0.25 [80%]	0.24 [78%]	0.25	N/A	0.18	0.24	2.05	6.78	N/A
1st Sym. bending	0.26 [95%]	0.26 [94%]	0.26	0.28	0.24	0.25	1.54	1.01	2.39
2nd Sym. bending	0.40 [93%]	0.41 [91%]	0.41	0.48	0.36	0.4	7.4	4.63	1.75
2nd Asym. bending	0.68 [N/A]	0.68 [N/A]	N/A	N/A	N/A	N/A	3.19	2.41	N/A
3rd Sym. bending	0.88 [92%]	0.85 [99%]	0.84	0.96	0.77	0.84	3.16	3.11	0.8
<i>Torsion</i>									
1st Torsion	0.45 [99%]	0.44 [92%]	0.49	0.52	0.44	0.44	1.96	1.74	1.27
2nd Torsion	0.70 [91%]	0.70 [98%]	0.68	0.78	0.60	0.60	2.28	5.17	1.27
3rd Torsion	1.09 [N/A]	1.09 [N/A]	N/A	N/A	N/A	N/A	1.12	1.15	N/A
<i>Longitudinal</i>									
1st Longitudinal	0.69 [N/A]	0.67 [N/A]	N/A	N/A	N/A	N/A	4.13	4.59	N/A
<i>Transverse</i>									
1st Sym. bending	0.12 [N/A]	0.12 [N/A]	N/A	N/A	N/A	N/A	2.41	5.92	N/A
1st Asym. bending	0.37 [N/A]	0.38 [N/A]	N/A	N/A	N/A	N/A	2.56	0.36	N/A
2nd Sym. bending	0.51 [N/A]	0.50 [N/A]	0.44	N/A	0.41	N/A	2.25	0.36	N/A
3rd Sym. bending	0.57 [N/A]	0.56 [N/A]	0.56	N/A	0.53	N/A	0.72	2.33	N/A

Note: N/A: not available.

*Value in [] denotes the MAC value between identified modes and their FEM fixed model counterparts.

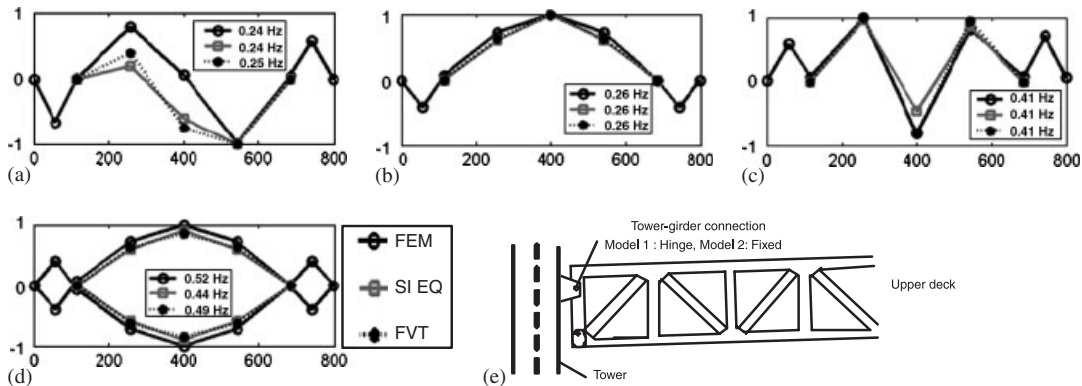


Figure 8. Representative mode shapes of girder portion of the Rainbow Bridge identified from MS2 response: (a) first vertical asymmetric; (b) first vertical symmetric; (c) second vertical symmetric; and (d) first torsion mode. (Note: SI EQ, system identification using earthquake records.) (e) Two connection models used for comparison.

analytical models (Table IV), one can observe that for the records applied in this analysis the fixed connection model is more accurate in representing the bridge than the hinge connection model. The natural frequencies obtained from seismic records are generally lower than those

Table V. Identified natural frequencies and damping ratios of the Tsurumi Fairway Bridge from the main shock of the Chuetsu-Niigata earthquake (MS1) and comparisons with results from other tests.

Mode	Natural frequency (Hz)						Damping ratio (%)				
	Identified						Identified				
	MS1-1 [MAC]*	MS1-2 [MAC]*	MS1-3 [MAC]*	AVT [25]	FVT [25]	FEM	MS1-1	MS1-2	MS1-3	AVT [25]	FVT [25]
<i>Longitudinal</i>											
1st Long.	0.19	—	—	—	—	—	1.15	—	—	—	—
<i>Vertical bending</i>											
1st Sym	0.21 [99%]	0.21 [97%]	0.21 [98%]	0.22	0.21	0.21	2.09	0.95	0.65	1.43	1.91
1st Asym.	0.30 [91%]	0.30 [92%]	0.30 [95%]	0.32	0.29	0.29	1.41	2.18	0.42	1.12	0.48
2nd Sym.	0.53 [95%]	0.53 [90%]	0.54 [91%]	0.54	0.52	0.51	4.49	0.32	1.76	0.48	1.75
2nd Asym.	0.61 [90%]	0.61 [91%]	0.61 [89%]	0.61	0.60	0.60	4.79	0.78	1.18	0.48	0.48
3rd Sym.	0.69	0.70	0.70	—	—	N/A	4.15	1.09	1.48	—	—
<i>Torsion</i>											
1st Torsion	—	0.54 [89%]	0.56 [91%]	0.56	0.54	0.50	—	1.28	2.59	0.80	1.12
2nd Torsion	0.81	0.79	0.81	—	—	N/A	2.35	3.15	1.89	—	—
3rd Torsion	1.57	1.57	1.57	—	—	N/A	1.49	2.23	2.67	—	—
<i>Transverse</i>											
1st Sym. towers in phase	0.29 [90%]	0.29 [89%]	0.29 [89%]	0.30	—	0.25	1.04	0.94	2.50	0.80	—
1st Sym towers out of phase	0.41	0.41	—	—	—	N/A	4.32	2.70	—	—	—
1st Asym towers out of phase	0.73	0.73	0.73	—	—	N/A	5.86	3.04	3.19	—	—
1st Asym. towers in phase	0.78	0.80	0.78	—	—	N/A	4.62	1.92	3.60	—	—
2nd Asym. towers out of phase	—	0.83	0.83	—	—	N/A	—	1.07	1.63	—	—
2nd Asym. towers in phase	0.86	0.88	0.86	—	—	N/A	3.99	2.98	3.62	—	—

Note: N/A: not available; — : not identified.

*Value in [] denotes the MAC value between identified modes and their FEM counterparts.

obtained from both AVT and FVT, suggesting an increased flexibility of the bridge during larger excitations.

5.3. Results of the Tsurumi Fairway Bridge

Fifteen modes within the frequency range of 0.19–1.57 Hz were identified consisting of eight vertical modes, six transverse modes, and one longitudinal mode (Table V). The lowest mode was the first swing longitudinal mode identified at 0.19 Hz, whereas the first vertical mode was a symmetrical bending identified at 0.21 Hz. The first transverse mode was identified at 0.29 Hz, where both towers were in phase with each other and also with the transverse motion of the girder. In the second transverse mode, identified at 0.41 Hz, both towers were out of phase. For the third and fourth modes, the girder revealed a typical first asymmetric bending pattern. The difference between the two was that in the third mode both towers were out of phase with each other, whereas in the fourth mode both towers were in phase. The modal damping ratios of the 15 modes were

identified within the range of 0.3–5.8%. The MAC values listed in Table V show that most of the identified modes are in very good agreement with the FEM modes. Note that the frequency estimates obtained from SI are relatively similar and consistent with the results of AVT and FVT [25]. These results are reasonable considering that the levels of ground motions are quite small and comparable to the level of ambient response.

6. TIME VARIATION OF MODAL PARAMETERS

The availability of various levels of input ground motions enables us to observe variations of modal parameters with respect to the amplitude of input acceleration. For this purpose, the inputs were bandpass filtered for a specified frequency range that encompasses the frequencies where each mode was identified. This procedure was employed to ensure that only the input responses within the corresponding frequency range of interest were included in the comparison.

6.1. Amplitude dependence of damping ratio

Figure 9 shows the typical variation of the damping ratio of the Yokohama Bay Bridge with respect to input amplitude plotted together with the results from six previous earthquakes [23]. The RMS of the bandpass-filtered input accelerations vary from 0 to 1.0 cm/s^2 , while the damping ratios vary from 0.5 to 5%. From this figure, one can observe that the damping ratios increase as the RMS of the input acceleration increases for both the vertical and transverse modes. The damping increase might be due to the greater energy dissipation caused by friction at bearings that occur during large excitations. The similar trend was also observed in the Tsurumi Fairway Bridge. At this bridge, seven frames of seismic records were analyzed with the RMS of the input amplitudes varying from 0.2 to 0.8 cm/s^2 . The results shown in Figure 10 reveal that while natural frequencies and mode shapes remain constant, damping ratios exhibit an increasing trend as input amplitude increases.

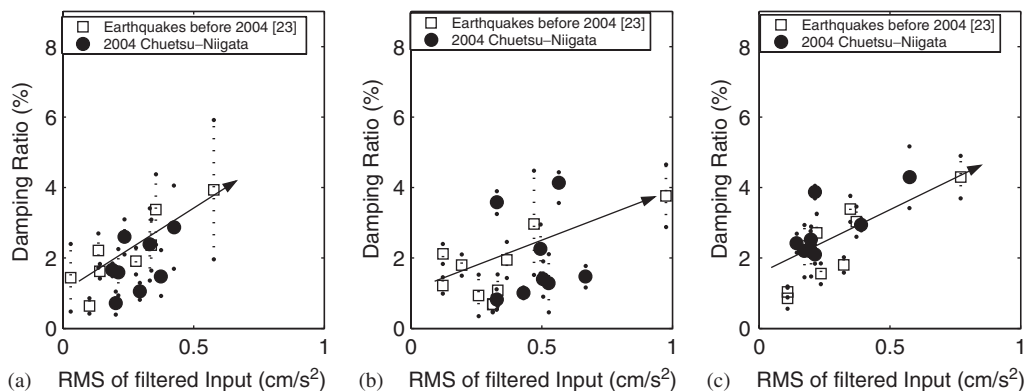


Figure 9. Variation of damping ratio of Yokohama Bay Bridge with respect to earthquake input amplitude: (a) first vertical bending mode; (b) second vertical bending mode; and (c) first transverse mode.

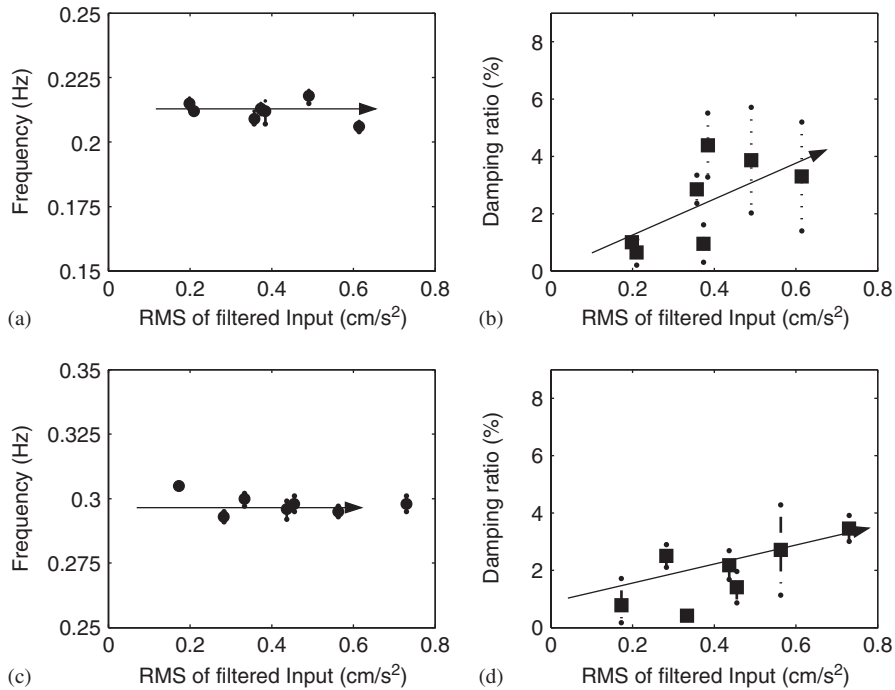


Figure 10. Variation of natural frequencies and damping ratios of Tsurumi Fairway Bridge identified from 2004 Chuetsu-Niigata earthquake: (a) frequency of first vertical bending mode; (b) damping of first vertical bending mode; (c) frequency of second vertical bending mode; and (d) damping of second vertical bending mode.

6.2. Amplitude dependence of the longitudinal mode of the Yokohama Bay Bridge

In addition to global behavior such as amplitude dependence of the damping ratios, variations of local components were also observed. The SI results of the Yokohama Bay Bridge revealed two types of the first longitudinal mode, where the main difference was the relative modal displacement between the end piers and girder. In design, the end piers and girder are connected by link-bearing connections (LBC) (Figure 11) whose essential function is to prevent the large inertial force of a superstructure from being imparted to substructures during large excitation. For this purpose, the LBC is expected to function as a longitudinal hinge connection to indicate that the girder and pier caps work as separate units. Thus, it is modeled in this way in FEM.

It should be noted that longitudinal girder motion induces nonlinear behavior of LBC. Moreover, since the longitudinal mode is excited only during earthquakes and is not measurable during either AVT or FVT, observation of its characteristics using seismic records may provide an opportunity to investigate the actual performance of LBC. To quantify relative modal displacement at the position of pier cap and girder, an index (γ) is calculated:

$$\gamma = \left| \frac{\phi_{\text{girder}} - \phi_{\text{pier cap}}}{\phi_{\text{girder}}} \right| \quad (18)$$

SYSTEM IDENTIFICATION APPLIED TO LONG-SPAN CABLE-SUPPORTED BRIDGES

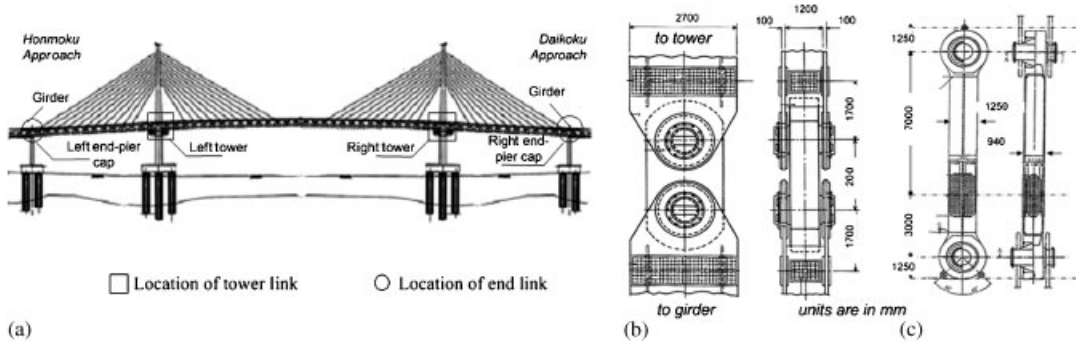


Figure 11. (a) Location of link-bearing connection of Yokohama Bay Bridge; (b) typical LBC at the tower; and (c) typical LBC at end piers.

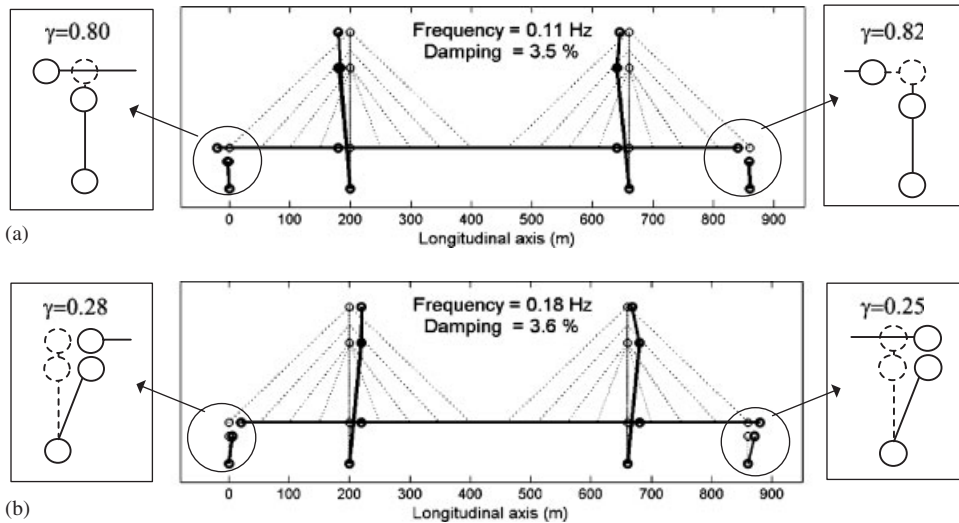


Figure 12. Two typical first longitudinal modes of Yokohama Bay Bridge identified from MSI response: (a) hinged-hinged mode: $\gamma_{\text{left}} = 0.80$, $\gamma_{\text{right}} = 0.82$ and (b) fixed-fixed mode: $\gamma_{\text{left}} = 0.28$, $\gamma_{\text{right}} = 0.25$.

where ϕ denotes the modal displacement normalized to unity for the maximum value. Equation (18) indicates that when the gap between pier cap and girder is large, the value of index (γ) is closer to unity.

The first type of longitudinal mode was identified from MS1-1, MS1-2, and MS2-1 with the frequencies between 0.11 and 0.15 Hz. It exhibited a large relative modal displacement as evidenced by $\gamma = 0.80$ and 0.82 for the left and right end piers, respectively (Figure 12(a)). The shape characteristics and frequency of this mode were very close to that of the FEM first longitudinal mode. The large relative modal displacement suggested that the hinge mechanism might have had occurred. The other mode was identified from MS1-3, MS2-2, and MS2-3 with the frequencies between 0.18 and 0.24 Hz (Figure 12(b)). The smaller relative modal displacements between end

piers and girder of this mode (i.e. $\gamma=0.28$ and 0.25 for the left and right end piers, respectively) suggested that the LBCs had yet to function as full-hinged connections, causing stiffer connection with higher natural frequency. These results indicate that performance of LBC depends on the amplitude of earthquake excitation and does not always follow the FEM prediction. Results of a more comprehensive observation of the LBC of the Yokohama Bay Bridge using seismic records and detail analysis are presented elsewhere [23].

7. CONCLUDING REMARKS

This paper has presented the application of SRIM-based SI to estimate modal characteristics of long-span cable-supported bridges using seismic records. Numerical investigations have shown that the SI works well in estimating modal parameters. The following conclusions can be drawn from the simulations:

- (1) There are two crucial factors in the estimation of modal parameters: model selection and p -value selection. Model selection is performed in a systematic way by eliminating the fictitious modes using successive threshold indicators. It is shown that due to noise in measurement, the actual minimum p -value is larger than the theoretical value, and can be determined from the convergent point in a typical plot of p -value *versus* identification error.
- (2) In the case of SI with an input–output scheme, frequency estimates are not influenced to any great degree by the nonstationarity of ground motion. On the contrary, errors in damping ratios increase when the system is subjected to narrowband nonstationary excitation. The scheme of output-only SI gives rather accurate results only for natural frequencies but not for damping estimates. Considering the possibility of nonstationary ground motions, these results emphasize the importance of input inclusion when using the identification scheme.

Applications of SI to three long-span cable-supported bridges in the Tokyo Bay Area using the 2004 Chuetsu-Niigata earthquake records have shown the efficiency of the method in estimating modal parameters. Observation from various levels of input ground motion reveals that while frequencies and mode shapes remain constant, damping ratios exhibit dependence on earthquake input amplitude, where the damping estimates increase as the amplitude of the input increases. The SI results also provide additional modal information and types of motion that could not be obtained during AVT and FVT. The effects of nonstationary seismic responses and ground accelerations in identification are small as evidenced by stabilized damping estimates especially with p -values larger than 200. This might be due to the long distance between the hypocenter of the earthquake and the bridges' sites, which makes the observed data become more stationary.

The benefits of the studied SI method are threefold: (1) it identifies modal parameters accurately with efficient use of relatively short earthquake records, (2) it is developed as a data-driven algorithm that requires no prior knowledge of structural information, and (3) it enables the identification of SIMO as well as MIMO systems, making it well suited for application to large and complex structures. In view of structural health monitoring, an efficient method of SI using seismic response is essential for quick assessment after earthquakes and for the application of modal-based damage detection methods.

ACKNOWLEDGEMENTS

The first author gratefully acknowledges the Japanese Ministry of Education, Culture, Sports, Science and Technology and the Japan Society for the Promotion of Science (JSPS) for the scholarship and fellowship provided during the study and this research. We express our gratitude to the Tokyo Metropolitan Expressway Public Corporation for providing motion records and construction drawings as well as to two anonymous reviewers for providing constructive comments and discussions throughout the review process. Any opinions, findings, and conclusions expressed in this material are those of the authors and do not necessarily reflect those of the Tokyo Metropolitan Expressway Public Corporation.

REFERENCES

1. Fujino Y, Kikkawa H, Namikawa K, Mizoguchi T. Seismic retrofit design of long-span bridges on metropolitan expressways in Tokyo. *Proceeding of the 6th International Bridge Engineering Conference*, Transportation Research Board, Boston Mass, U.S.A., 2005.
2. Abdel-Ghaffar AM, Scanlan RH. Ambient vibration studies of the Golden Gate Bridge: I. Suspended structure. *Journal of Engineering Mechanics* (ASCE) 1985; **111**(4):463–482.
3. Abdel-Ghaffar M, Scanlan RH. Ambient vibration studies of the Golden Gate Bridge: II. Pier tower structure. *Journal of Engineering Mechanics* (ASCE) 1985; **111**(4):483–499.
4. Aktan AE, Catbas N, Turer A, Zhang Z. Structural identification: analytical aspect. *Journal of Structural Engineering* (ASCE) 1998; **124**(7):817–829.
5. Aktan AE, Farhey DN. Structural identification for condition assessment: experimental arts. *Journal of Structural Engineering* (ASCE) 1997; **123**(11):1674–1684.
6. Brownjohn JM, Dumanoglu AA, Severn RT, Blakeborough A. Ambient vibration survey of the Bosphorus suspension bridge. *Earthquake Engineering and Structural Dynamics* 1989; **18**:263–283.
7. Nagayama T, Abe M, Fujino Y, Ikeda K. Structural identification of non-proportionally damped systems and its application to a full scale suspension bridge. *Journal of Structural Engineering* (ASCE) 2005; **131**(10):1536–1545.
8. Siringoringo DM, Fujino Y. System identification of a suspension bridge from ambient vibration response. *Engineering Structures*, in press, DOI: 10.1016/j.engstruct.2007.03.004.
9. Werner SD, Beck JL, Levine MB. Seismic response evaluation of Meloland Road Overpass using 1979 imperial Valley Earthquake Records. *Earthquake Engineering and Structural Dynamics* 1987; **15**:249–274.
10. Chaudhary MTA, Abe M, Fujino Y, Yoshida J. System identification of two base-isolated bridges using seismic records. *Journal of Structural Engineering* (ASCE) 2000; **126**(10):1181–1194.
11. Arici Y, Mosalam KM. System identification of instrumented bridge systems. *Earthquake Engineering and Structural Dynamics* 2003; **32**:999–1020.
12. Smyth AW, Jin-Song P, Masri SF. System identification of the Vincent Thomas suspension bridge using earthquake records. *Earthquake Engineering and Structural Dynamics* 2003; **32**(3):339–367.
13. Pridham BA, Wilson JC. Identification of based-excited structures using output-only parameter estimation. *Earthquake Engineering and Structural Dynamics* 2004; **33**(1):133–155.
14. Lus B, Betti R, Longman RW. Identification of linear structural system using earthquake-induced record. *Earthquake Engineering and Structural Dynamics* 1999; **28**:1449–1467.
15. Juang JN. System realization using information matrix. *Journal of Guidance, Control, and Dynamics* 1997; **20**(3):492–500.
16. Juang JN. State-space system realization with input-and-output-data correlation. *NASA Technical Paper 3622*, April 1997.
17. Arici Y, Mosalam KM. Modal identification of bridge system using state-space method. *Structural Control and Health Monitoring* 2005; **12**:381–404.
18. Fleming JF, Egeseli EA. Dynamic behavior of a cable-stayed bridge. *Earthquake Engineering and Structural Dynamics* 1980; **8**:1–16.
19. Clough RW, Penzien J. *Dynamics of Structures* (2nd edn). McGraw-Hill: New York, 597–600.
20. Juang JN, Pappa RS. Effects of noise on modal parameters identified by Eigensystem Realization Algorithm. *Journal of Guidance, Control, and Dynamics* 1986; **9**:294–303.
21. The Yokohama Bay Bridge. Published by the Metropolitan Expressway Public Corporation, Tokyo, Japan, 1991; 164–172 (in Japanese).

22. Siringoringo DM, Fujino Y. Dynamic characteristics of a curved cable-stayed bridge identified from strong motion record. *Engineering Structures* 2007; **29**(8):2001–2017.
23. Siringoringo DM, Fujino Y. Observed dynamic performance of the Yokohama Bay Bridge from system identification using seismic records. *Journal of Structural Control and Health Monitoring* 2006; **13**(1):226–244.
24. Izumi K, Odagiri N, Ogiwara M, Yabe J, Ochiai M, Ohgaki K, Watanabe Y. Vibration test for a two hinge-double deck suspension bridge. *Journal of Japan Society of Civil Engineering* 1994; **40A**:721–733 (in Japanese).
25. Yamaguchi H, Takano H, Ogasawara M, Shimosato T, Kato M, Okada J. Identification of dynamic characteristics by field vibration test in Tsurumi Tsubasa Bridge. *Journal of Japan Society of Civil Engineering* 1996; **543**: 247–258 (in Japanese).